Development of a modified BEMT model for the analysis of helical bladed vertical axis tidal turbines

Mohammad Fereidoonnezhad, Seán B. Leen, Stephen Nash, Tomas Flanagan and Patrick McGarry

Abstract— **Classical blade element momentum theory (BEMT) formulations are not capable of accurately simulating complex blade geometries, such as spiral or helical blade geometries. In this paper, we develop a modified BEMT model to calculate hydrodynamic forces acting on the helical vertical axis tidal turbines. We validate the model using experimental data for a prototype VAWT. We then perform a parametric investigation of the effect of blade helix angle on the turbine performance. Our model predicts that an increase in blade helix angle results in reduced power fluctuations. Additionally, computed fluctuations in tangential and normal forces acting on blades are shown to reduce significantly with increasing blade helix angle, suggesting a reduction in risk of fatigue failure. Fluctuating hydrodynamic forces computed by our modified BEMT model are input into a finite element (FE) framework to compute the stress state in a fibre reinforced composite blade material for a range of blade azimuthal positions.**

Keywords— **Blade element momentum theory, Helical vertical axis tidal turbine, FEA Analysis.**

I. INTRODUCTION

TIDAL turbines can be categorized into two types based on their blade rotation axis: horizontal-axis turbines (HATT) and vertical-axis turbines (VATT). HATTs are installed on either a floating platform or on the seabed. Their design is similar to that of horizontal axis wind turbines (HAWT), but they are specifically optimized for the low velocity and high density of tidal currents. In contrast, VATTs have blades that rotate around a vertical axis, allowing them to capture energy from water currents that flow in any direction. These turbines are well-suited for use in areas such as tidal channels or locations where the water flow direction changes frequently.

Several studies have investigated the efficiency and effectiveness of wind and tidal turbine designs ([1-5]). The aerodynamic analysis of vertical axis wind turbines (VAWTs) and hydrodynamic analysis of VATTs have been studied using a range of approaches, including blade element momentum theory (BEMT) models [6-8], vortex and panel models [3], computational fluid dynamics models [9-12] and experiments [13].

BEMT is a widely used approach to analyse both VATT and HATT by modelling the hydrodynamic forces acting on each blade element. Glauert [14] originally introduced BEMT as an analysis method for propellers, while Templin [15] presented the first application of this approach to vertical axis turbines (VATs). This implementation used a single stream-tube approach in which the turbine was represented by a single actuator disc enclosed within the stream-tube.

In recent years, there has been significant progress in the development of BEM models for VATs. Mannion et al. [6] presented a BEMT model for high solidity and highly loaded VATT rotors, which overcomes the limitations of traditional BEMT models. The model incorporates correction factors to account for dynamic stall, flow expansion, and finite aspect ratios. Model

Sponsor and financial support acknowledgement: The research conducted in this paper was jointly funded by the Irish Research Council under grant number EPSPG/2022/245, and by ÉireComposites under the Horizon 2020 FTI CRIMSON project (Commercialisation of a Recyclable and Innovative Manufacturing Solution for an Optimised Novel marine turbine) (Grant number: 971209).

Mohammad Fereidoonnezhad is with Department of Mechanical and Biomedical Engineering, College of Science and Engineering, University of Galway, University Road, Galway H91 CF50, Ireland (e-mail: m.fereidoonnezhad1@universityofgalway.ie).

Sean B. Leen is with Department of Mechanical and Biomedical Engineering, College of Science and Engineering, University of Galway, University Road, Galway H91 CF50, Ireland (e-mail: sean.leen@universityofgalway.ie).

Stephen Nash is with Department of Civil Engineering, College of Science and Engineering, University of Galway, University Road, Galway H91 CF50, Ireland (e-mail: stephen.nash@universityofgalway.ie).

Tomas Flanagan is with ÉireComposites Teo., Údarás Industrial Estate An Choill Rua, Inverin, Galway, H91 Y923, Ireland (e-mail: t.flanagan@eirecomposites.com)

Patrick McGarry is with Department of Mechanical and Biomedical Engineering, College of Science and Engineering, University of Galway, University Road, Galway H91 CF50, Ireland (e-mail: patrick.mcgarry@universityofgalway.ie)

Digital Object Identifier: https://doi.org/10.36688/ewtec-2023-676

predictions were evaluated for both low and high solidity rotors.

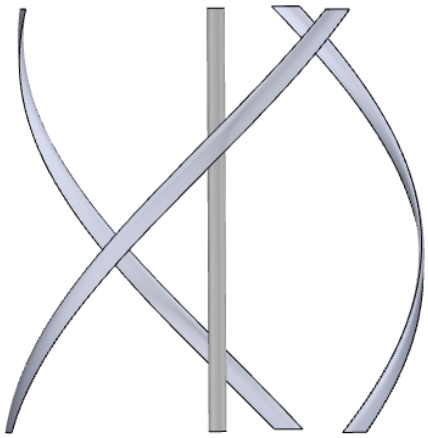

Fig. 1. Helical-bladed vertical axis turbine

Hydrodynamic analysis of a novel vertical axis tidal turbine concept using a BEMT adapted for the complex spiral geometry of the blades has been presented by Heavey et al. [7]. The authors considered a range of blade designs based on different rotor height to diameter ratios, leading to a range of hydrodynamic power curves with different optimal tip speed ratios and peak power levels. The Gorlov turbine design [16] consists of a vertical rotor with helically shaped blades that wrap around the central axis in a corkscrew-like pattern, as shown in Fig. 1.

Recent studies have utilized various computational models to assess the performance of vertical axis turbines with different blade shapes, including helical, Troposkien, V-shaped, and hybrid designs. This included both experimental investigations [17-19] and numerical studies using CFD approaches [5,20-23] to examine the hydrodynamic performance of VATTs. A classical BEMT approach, including stream tube models, has been employed to perform computationally efficient analysis and optimization of helical vertical axis turbines (HVAT) [25]. Mars et al. [24] conducted a study to examine the stress and deformation of vertical axis turbines with straight and helical blades using hydrodynamic and structural analysis models. The hydrodynamic forces and pressures on the turbines were computed using classical BEMT and CFD models. Simulations were performed to analyse a range of operating conditions, from start-up to over-speed conditions. Blade stress and deflection was analysed beam theory and finite element analysis.

Moghimi et al [25] used a classical BEMT approach for helical vertical axis wind turbines (HVAWT). It was concluded that increasing helical blade angle can decrease the fluctuation of the turbine and does not have a significant effect on power coefficient. However, a limitation of using the classical BEMT approach for curved blades is the underlying model assumption that the leading edge is orthogonal to the free-stream velocity. This assumption does not incorporate an accurate description of the blade geometry, even if high-concentration spatial discretisation is implemented.

In the present study, we develop a modified BEMT model for curved turbine blades that accounts for the changing orientation of the leading edge of the blade and the chord. We uncover a complex pattern of blade forces for helical bladed turbines, which we use as input to finite element structural analysis of a helical bladed VATT manufactured using a glass-fibre composite lay-up material.

II. MODEL DEVELOPMENT

A. *Development of a modified BEMT model for curved blades*

In this study we develop a modified BEMT, presented in vectorised form and implemented MATLAB, in order to accurately calculate blade hydrodynamic forces and torque for general curved blade designs. Fig.2 shows a schematic of the cross-section of a VATT, indicating the free-stream velocity (U_∞), turbine angular velocity (ω), azimuthal angle (θ), relative velocity (W), angle of attack (α), lift force (F_L), drag force (F_D), normal force (F_N), tangential force (F_T).

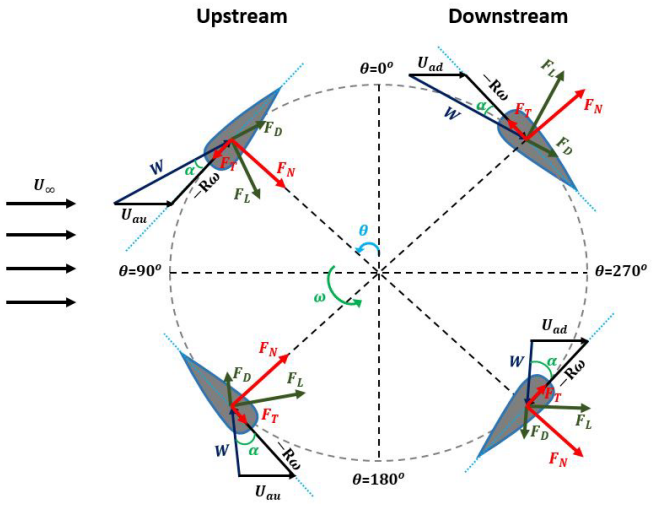

Fig. 2. Cross-section of a VATTT

Fig. 3 shows a schematic of a curved blade where the leading edge is not orthogonal to the freestream velocity. The chord vector ($\vec{c}$) and blade direction vector ($\vec{s}$) are shown. In case (a) the chord is orthogonal to the leading edge, such that the chord does not lie in the r-θ plane. In case (b) the chord lies in the r-θ plane. Finally, for comparison, case (c) shows the geometric approximation required to use the classical BEMT approach for a curved blades, such that leading edge is

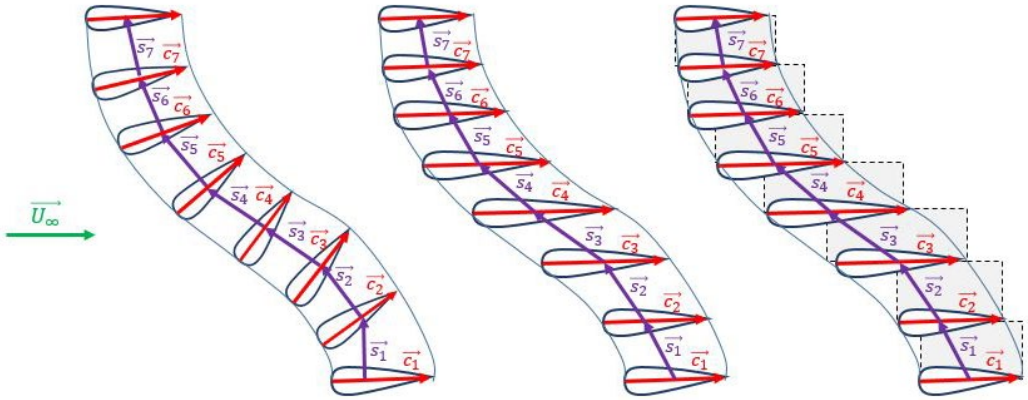

Fig. 3: A schematic of a curved blade (a) with chord orthogonal to leading edge (b) Modified BEMT for blade with chord in $r-\theta$ plane (c) Classic BEMT simplification for curved bladed with chord in $r-\theta$ plane

assumed to be orthogonal to the freestream velocity as part of the geometric discretisation.

In our modified BEMT model we first define a general expression for the chord vector ($\vec{c}$) and blade direction vector ($\vec{s}$) in a Cartesian co-ordinate system in equations (1) and (2),

$$\vec{c} = c_0 \sin\delta \cos\theta\, \vec{\imath} + c_0 \sin\delta \sin\theta\, \vec{\jmath} + c_0 \sin\delta\, \vec{k} \quad (1)$$

$$\vec{s} = -s_0 \cos\delta \cos\theta\, \vec{\imath} - s_0 \cos\delta \sin\theta\, \vec{\jmath} + s_0 \sin\delta\, \vec{k} \quad (2)$$

where c_0 is the magnitude of the chord, s_0 is the length of each element and δ is the angle between blade direction vector and x-y plane.

The radial vector for a point on the turbine blade is given as

$$\vec{r} = -R \sin\theta\, \vec{\imath} + R \cos\theta\, \vec{\jmath} \quad (3)$$

where R is the magnitude of turbine radius.

The angular velocity is given as:

$$\vec{\omega} = TSR\left(\frac{|\vec{U_\infty}|}{|\vec{r}|}\right)\vec{k}. \quad (4)$$

The tangential velocity is given as:

$$\vec{V_t} = \vec{\omega} \times \vec{r} = -|\vec{r}||\vec{\omega}| \cos\theta\, \vec{\imath} - |\vec{r}||\vec{\omega}| \sin\theta\, \vec{\jmath} \quad (5)$$

The upstream velocity is given as:

$$\vec{U_a} = (1-a)\vec{U_\infty}. \quad (6)$$

The relative velocity, which is a summation of flow velocity and angular velocity, is given as:

$$\vec{W} = \vec{U_a} - \vec{V_t} = \left(U_{a_x} + |\vec{r}||\vec{\omega}|\, cos\,\theta\right)\vec{\imath} + \left(U_{a_y} + |\vec{r}||\vec{\omega}|\, sin\,\theta\right)\vec{\jmath} + \left(U_{a_z}\right)\vec{k}. \quad (7)$$

The angle of attack is the angle between the relative velocity and chord vectors, and is given as:

$$\begin{cases} \alpha = tan^{-1}\left(\dfrac{\vec{W}\times\vec{c}}{\vec{W}.\vec{c}}\right) & for\ Upstream \\ \alpha = -tan^{-1}\left(\dfrac{\vec{W}\times\vec{c}}{\vec{W}.\vec{c}}\right) & for\ Downstream \end{cases} \quad (8)$$

The drag unit vector ($\vec{e_D}$) and relative velocity unit vector ($\vec{e_W}$) are parallel. Lift and drag unit vectors are orthogonal ($\vec{e_D}.\vec{e_L} = 0$). We can also generalise that the blade unit vector is orthogonal to the lift vector ($\vec{e_s}.\vec{e_L} = 0$). Using these two conditions, the lift and drag unit vectors are given as:

$$\vec{e_D} = \vec{e_W} = \frac{\vec{W}}{\|\vec{W}\|} \quad (9)$$

$$\vec{e_L} = \vec{e_D} \times \vec{e_s}. \quad (10)$$

We can now calculate the lift and drag forces from:

$$\vec{F_L} = \left(\frac{1}{2}\rho C_L \|\vec{c}\times\vec{s}\|(\vec{W}.\vec{W})\right)\vec{e_L} \quad (11)$$

$$\vec{F_D} = \left(\frac{1}{2}\rho C_D \|\vec{c}\times\vec{s}\|(\vec{W}.\vec{W})\right)\vec{e_D} \quad (12)$$

where $\|\vec{c}\times\vec{s}\|$ is the area of a discretised blade element. Thus, the total force acting on the blade is given as:

$$\vec{F_{tot}} = \vec{F_L} + \vec{F_D}. \quad (13)$$

The tangential force is given as:

$$\vec{F_T} = (\vec{F_{tot}}.\vec{e_{V_t}})\vec{e_{V_t}}, \quad (14)$$

where $\vec{e_{V_t}} = \frac{\vec{V_t}}{\|\vec{V_t}\|}$ is the tangential velocity unit vector, and the normal force vector is given as:

$$\vec{F_N} = (\vec{F_{tot}}.\vec{e_r})\vec{e_r}. \quad (15)$$

The torque acting on the blade is obtained from:

$$\vec{Q} = \vec{r} \times \vec{F_T}. \tag{16}$$

The power coefficient is given as:

$$C_p = \frac{Q_{avg}}{0.5\rho A {U_\infty}^2} \tag{17}$$

where Q_{avg} is the average torque acting on the rotor.

B. *Calculation of induction factors*

The single stream tube (SST) model was first proposed by Templin [15]. This model encloses the entire turbine within a single stream tube. The multiple stream tube (MST) model, developed by Strickland [26], employs several parallel and adjacent stream tubes. The double multiple stream tube (DMST) model [27], shown in Fig.4, overcomes the limitations of the MST model by distinguishing between the upstream and downstream regions of the turbine.

As shown in Fig.4, the actuator disc is divided into two sections representing the upstream and downstream regions. The induced velocities for each stream tube in the upstream and downstream regions are represented by U_{au} and U_{ad}, respectively.

The relationship between upstream induced velocity (U_{au}), equilibrium induced velocity (U_e) and downstream induced velocity (U_{ad}), is given as follows:

$$\begin{aligned} \overrightarrow{U_{au}} &= a_u \overrightarrow{U_\infty} \\ \overrightarrow{U_e} &= (2a_u - 1)\overrightarrow{U_\infty} \\ \overrightarrow{U_{ad}} &= (2a_u - 1)a_d \overrightarrow{U_\infty} \end{aligned} \tag{18}$$

where a_u and a_d are the upstream and downstream induction factors, respectively.

Through an iterative process the induction factor is obtained from the following expression:

$$a = KK_0/KK_0 + \int_{\theta-\frac{\Delta\theta}{2}}^{\theta+\frac{\Delta\theta}{2}} f(\theta)d\theta \tag{19}$$

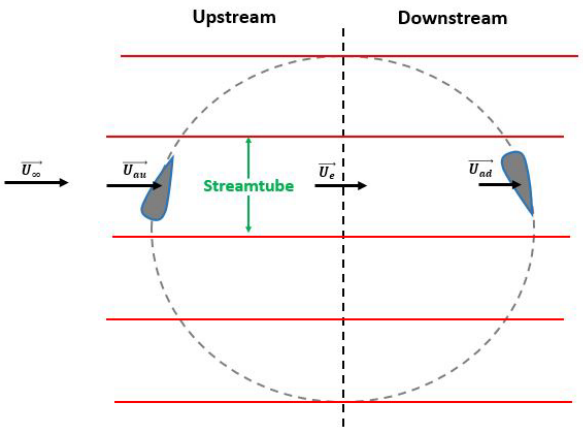

Fig. 4: Double multiple streamtube model

where $K = 8\pi R/Nc$ is a geometrical parameter for the rotor and:

$$f(\theta) = \left(\frac{\overrightarrow{W}}{\overrightarrow{U_a}}\right)^2 [C_T \cos\theta - C_n \sin\theta] \tag{20}$$

$$K_0 = cos\left(\theta + \frac{\Delta\theta}{2}\right) - cos\left(\theta - \frac{\Delta\theta}{2}\right). \tag{21}$$

The value of K_0 is directly linked to the width of each streamtube, where the streamtube width is equal to K_0 multiplied by the rotor radius.

In the trivial case of $\delta = 90^o$ and $\phi = 0^o$, our model collapses to the case of a straight bladed VAWT with a horizontal chord in the r-θ plane, and a leading edge that is orthogonal to the freestream velocity. As expected, our modified BEMT model computes identical results to the classical BEMT approach (see Appendix A) for this simple case, with computed normal and tangential forces providing a reasonable approximation of experimentally measured trends [28], as shown in Fig. 5.

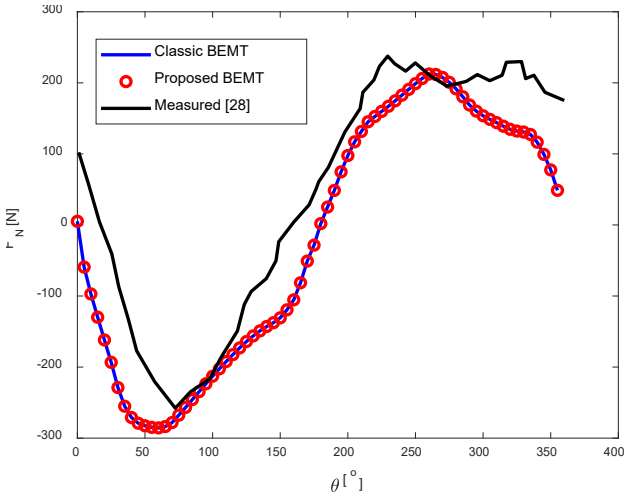

(a)

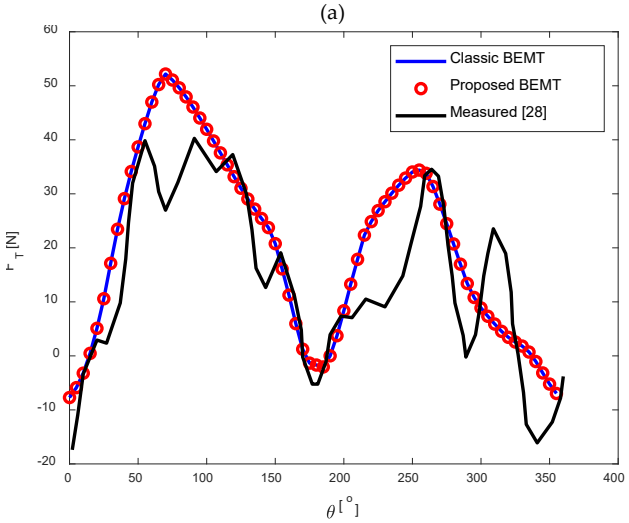

(b)

Fig. 5. (a): Normal force (F_N) and (b): tangential force (F_T) acting on a straight bladed VAWT at TSR =3.59. Blades have a NACA

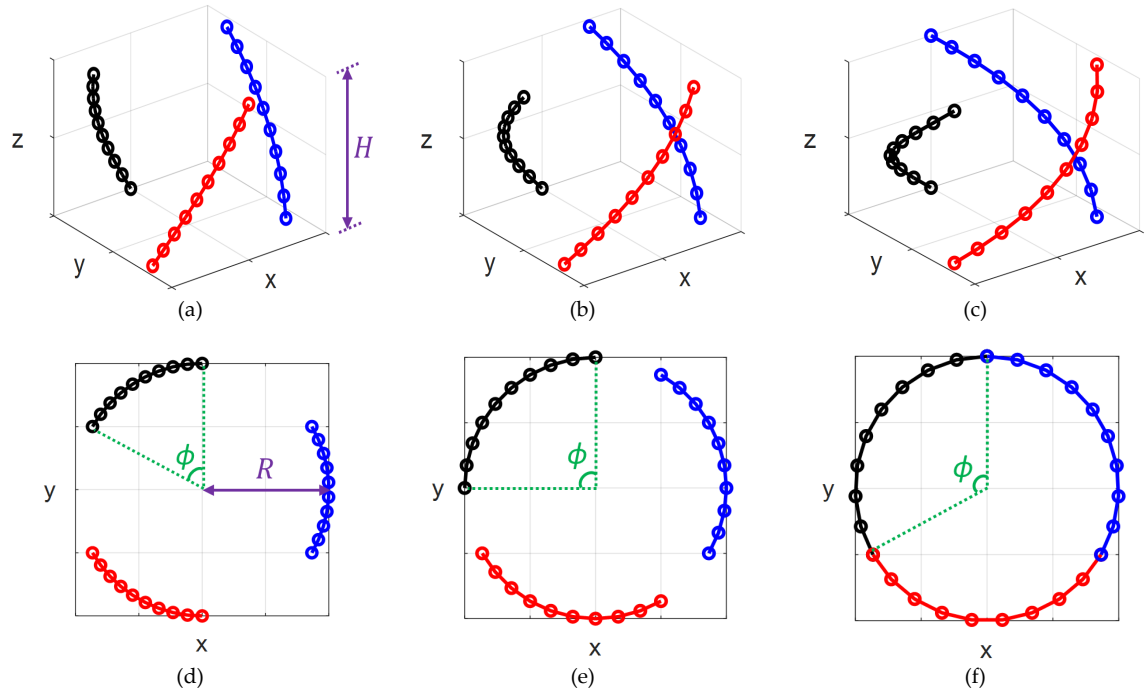

Fig. 6. Isometric and top views of helical blade geometry at various helical angles; (a) and (d):ϕ= 60^o, (b) and (e): ϕ = 90^o, (c) and (f): ϕ = 120^o

0021 airfoil profile and a chord length of 0.25 m. The turbine has a diameter of 6 m and a height of 5 m.

III. BEMT RESULTS FOR HELICAL TURBINES

We use our modified BEMT model to analyse the performance of helical bladed turbines. We firstly develop a MATLAB code to parameterise the design of helical bladed VATTs. Fig. 6 presents isometric views (a-c) and corresponding plan views (d-f) of the centre lines of three-bladed VATTs with helix angles, ϕ, of 60^o, 90^o and 120^o.

Reference turbine parameters and operational conditions are presented in Table I. The lift and drag coefficients for NACA0018 at different Reynolds numbers [29] are used as inputs to the modified BEMT model.

TABLE I
HELICAL VATT DESIGN PARAMETERS

Symbol	Design Parameters	Values
N_B	Number of blades	3
-	Blade hydrofoil	NACA0018
ϕ	Helical blade angle	120^o
TSR	Tip speed ratio	3
ω	Angular velocity	2.67 rad/s
U_∞	Free stream velocity	2 m/s
ρ	Water density	1000 kg/m^3

Fig. 7 presents the turbine power curve (C_p versus TSR) as a function of helix angle, ϕ. Two cases are considered for each helix angle: (i) the chord lies in the r-θ plane (i.e. the chord is assumed to be horizontal); (ii) the chord is orthogonal to the leading edge. For case (i), the peak power output for helix angles of ϕ = 30^o and ϕ = 60^{o}are slightly higher than that for a straight bladed turbine (ϕ = 0^o), with a slight decrease in power computed for ϕ = 90^o and ϕ = 120^o.

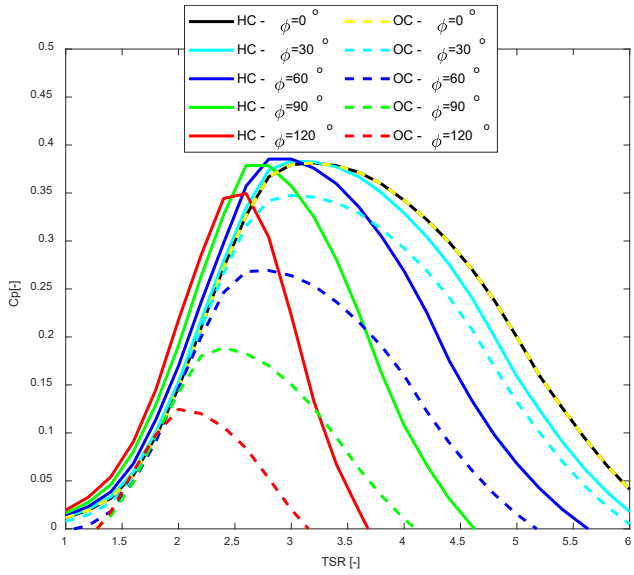

Fig. 7. Power curve for helical blade turbine with chord orthogonal to leading edge (OC) and chord in r-θ plane (Horizontal chord (HC))

Next, considering case (ii), significantly lower power is generated when the chord is orthogonal to the leading edge. As $\vec{c}$ is not aligned with $\overrightarrow{U_\infty}$, an increase in ϕ results in a reduction of a component of $\overrightarrow{U_\infty}$ that generates lift.

Fig. 8 shows the normal and tangential force vectors for a section at the bottom of the blade during a blade rotation for a helix angle of 120^0. In this context, the non-dimensional values along the x and y directions are denoted as $\bar{x}$ and $\bar{y}$, respectively, and are defined as $\bar{x} = \frac{x}{R}$ and $\bar{y} = \frac{y}{R}$, where R represents a turbine radius. The

magnitude of the normal force is lower downstream compared to its values upstream. The magnitude of tangential force monotonically increases from $\theta = 0^o$ to $\theta = 90^o$. Thereafter, the angle of attack enters the stall region, leading to a rapid decrease in tangential force and torque.

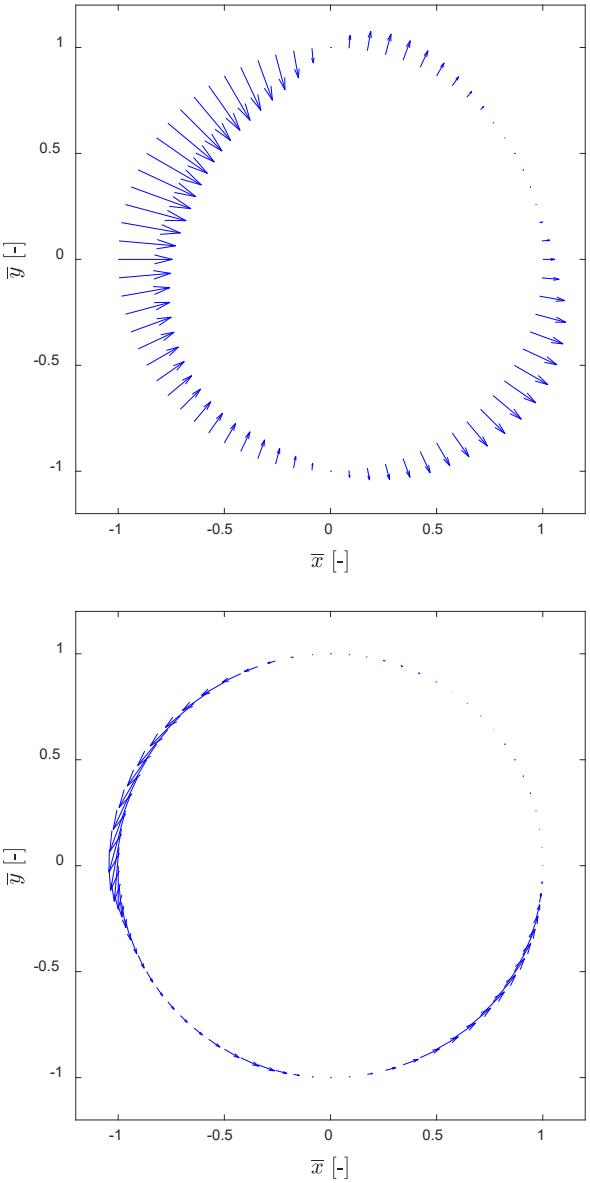

Fig. 8. Normal (Top) and Tangential force vectors (Bottom)

Fig. 9 shows the total tangential force acting on a blade as a function of azimuthal position (θ) at TSR corresponded to the maximum power coefficient (TSR=3.6 for straight bladed, and TSR=3.4, 3.2, 2.8 and 2.8 for $\phi = 0^0, 30^0, 60^0, 90^0$ and 120^0 respectively).

At the downstream, due to the effect of induction factor (Fig. 10) the torque value is almost zero, and the blade does not create any lift force.

A higher helix angle reduces the duration for which zero force occurs because a lower fraction of the blade length will be in the stall-regime at a given time-point.

In contrast, a straight blade experiences negligible tangential force for over half of the blade rotation.

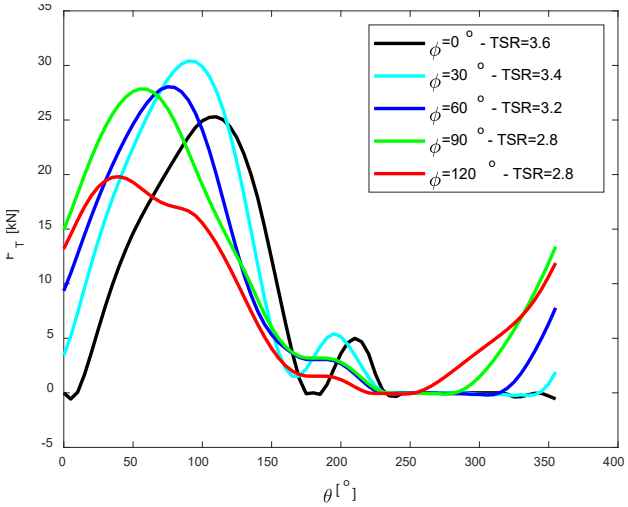

Fig. 9. Total tangential force acting on a single blade as a function of azimuthal position

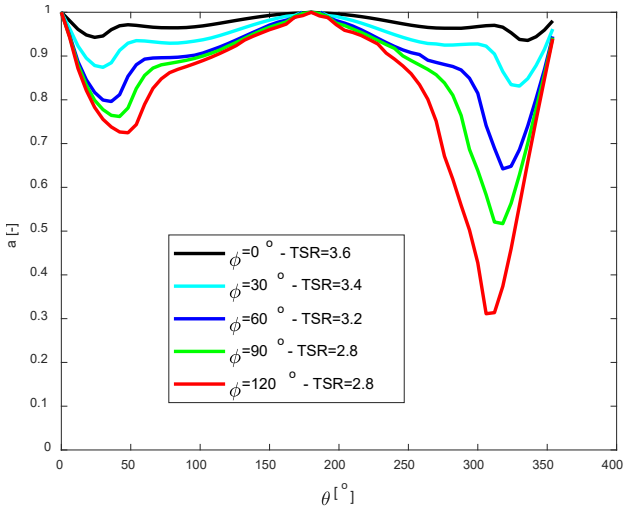

Fig. 10. Upstream and downstream induction factor for various helical blade angle

However, peak tangential force reduces with increasing helix angle because a lower fraction of the blade will be at a favourable angle of attack to generate high lift forces at a given time-point.

Fig. 10 displays the upstream and downstream induction factors as defined in equation (18). An increase in helical angle,ϕ, results in a higher level of disruption of the downstream flow. Therefore, an increase in ϕ leads to a decrease in the induction factor, as shown in Fig. 10 and a decrease in the torque generated by the turbine, as shown in Fig. 9.

A shown in our modified BEMT calculations of torque coefficient, C_Q, as a function of azimuthal angle, the mean torque coefficient over a turbine rotation, $\overline{C_Q}$, is lower for $\phi = 120^0$ ($\overline{C_Q}$=0.113) than for $\phi = 60^0$ ($\overline{C_Q}$=0.127) and $\phi = 90^0$ ($\overline{C_Q}$=0.143). The mean torque for a straight bladed turbine ($\phi = 0^0$) ($\overline{C_Q}$=0.103) is lower to that computed for $\phi = 120^0$. This demonstrates that an optimal value of ϕ can be identified in order to optimise torque and power output.

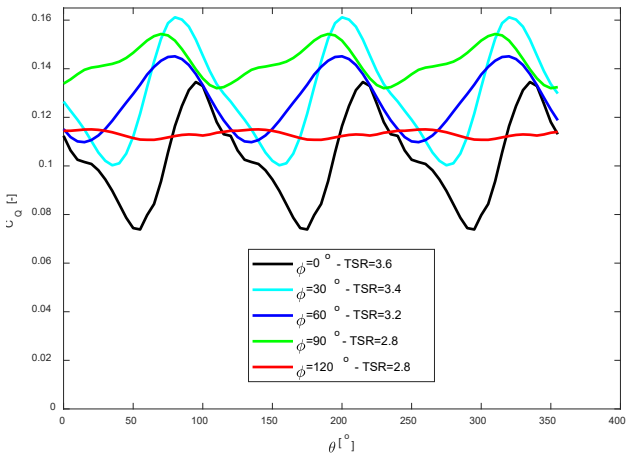

Fig. 11. Torque acting on the 3blades

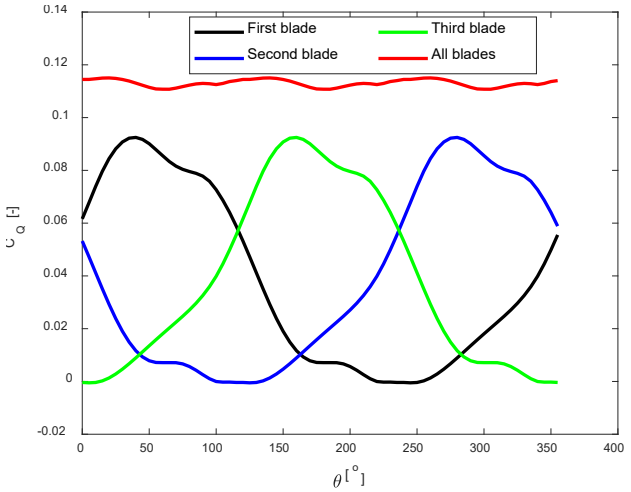

Fig. 12. Torque coefficient as a function of azimuthal position

As shown in Fig. 11, an increase in helical angle, ϕ, results in a reduction in torque fluctuation over a turbine rotation. Again, at any given time-point a blade with high ϕ will occupy a higher range of azimuthal positions over the length of the blade, so that a wider range of tangential forces act on the blade. As shown in Fig. 12, the total torque coefficient for the turbine is given as the summation of C_Q for the three blades, which are identical, but out of phase by 120^0 for a three-bladed turbine. Such a reduction in torque fluctuation presents significant advantages in terms of turbine design and performance. Firstly, a reduction in fluctuation of power output is desirable. Secondly, a reduction in load fluctuation during a rotation can potentially reduce the risk of fatigue failure of the blade.

Fig. 13 shows the computed tangential and normal forces acting along the length of helical blade ($\phi = 120^0$) for three blade positions, represented by the azimuthal position of the bottom of the blade (θ_0). The non-dimensional value along the length of blade is denoted as $\bar{s}$ and is defined as $\bar{x} = \frac{s}{L}$. During a complete rotation, a blade can experience a wide range of load patterns with significant variations in force along the length of the blade.

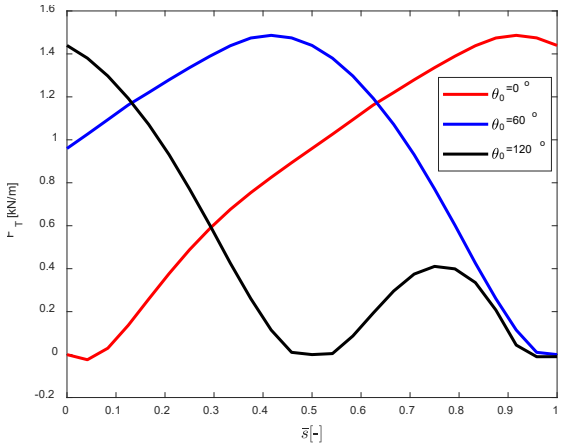

Fig. 13. Tangential forces acting on a single blade

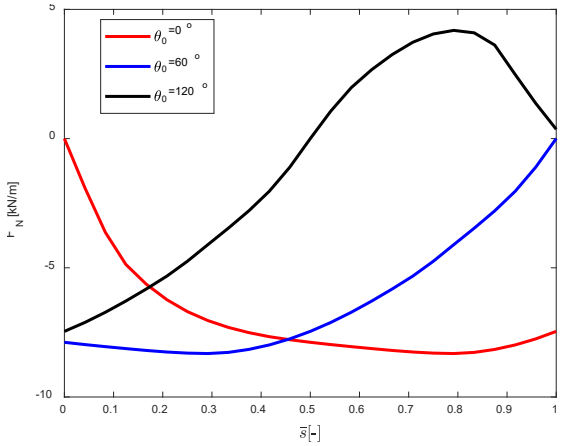

Fig. 14. Normal forces acting on a single blade

As an example, for $\theta_0 = 60^o$, F_T increases from 0.96 kN/m at the bottom of the blade ($\bar{s} = 0$), increasing to a peak of 1.49 kN/m at $\bar{s} = 0.42$, and then decreasing to 0 kN/m at the top of the blade ($\bar{s} = 1$). Similarly, the normal force,F_N, is negative (inwards in the radial direction) at the bottom of the turbine ($\bar{s} = 0$), and then decreases to a minimum of $F_N = -8.32$ kN/m at $\bar{s} = 0.30$, followed by an increase to a value of $F_N = 0$ kN/m at the top of the blade ($\bar{s} = 1$).

IV. STRUCTURAL ANALYSIS OF HELICAL BLADE

The complex distributions of normal and tangential forces computed using our modified BEMT model are applied to a finite element structural analysis of a helical blade ($\phi = 120^0$) in order to compute deflections and stress distributions throughout the blade. Analyses are performed using the Abaqus/Standard (implicit) software.

C. *Blade material and boundary conditions*

Fibre reinforced composite materials especially, glass fibre reinforced polymer (GFRP) and carbon fibre reinforced polymer (CFRP) are widely preferred for the construction of large wind and tidal turbine blades [30, 31]. We assume that the blade is composed of a composite material comprising of 20 plies. There are two tri-axial plies allocated for each of the upper and lower surfaces, while the middle section consists of 16

TABLE II
PROPERTIES OF MATERIALS USED IN THE CURRENT STUDY [33]

	$E_1\,[MPa]$	$E_2\,[MPa]$	$E_3\,[MPa]$	$G_{12}\,[MPa]$	$G_{13}\,[MPa]$	$G_{23}\,[MPa]$	ν_{12}	ν_{13}	ν_{23}
UD	39700	11900	11900	3670	3670	3670	0.2	0.2	0.2
TRI	21477	13530	12041	9126	3670	3670	0.49	0.12	0.15

unidirectional plies. The material properties for unidirectional (UD) and tri-axial (TRI) fibre orientation used in this study are given in Table II [33]. Each ply has a thickness of 0.5 mm, resulting in a composite blade thickness of 10 mm.

End-constraints are applied to the blade, and the distribute normal (Fig. 13) and tangential forces (Fig. 14) computed using our modified BMET model are applied.

D. *Finite Element Analysis Results*

Fig. 15(a) shows the complex patterns of blade radial deflection for three azimuthal positions. In all cases, the blade transitions from inwards (negative) deflection to positive (outwards deflection). A maximum inwards deflection ($u_r = 31.35\,mm$) and outwards deflection ($u_r = 30.41\,mm$) are computed for $\theta_0 = 120^0$. Given that the computed blade deflections are of the order of 1×10^{-3} times the turbine radius, our analyses suggest

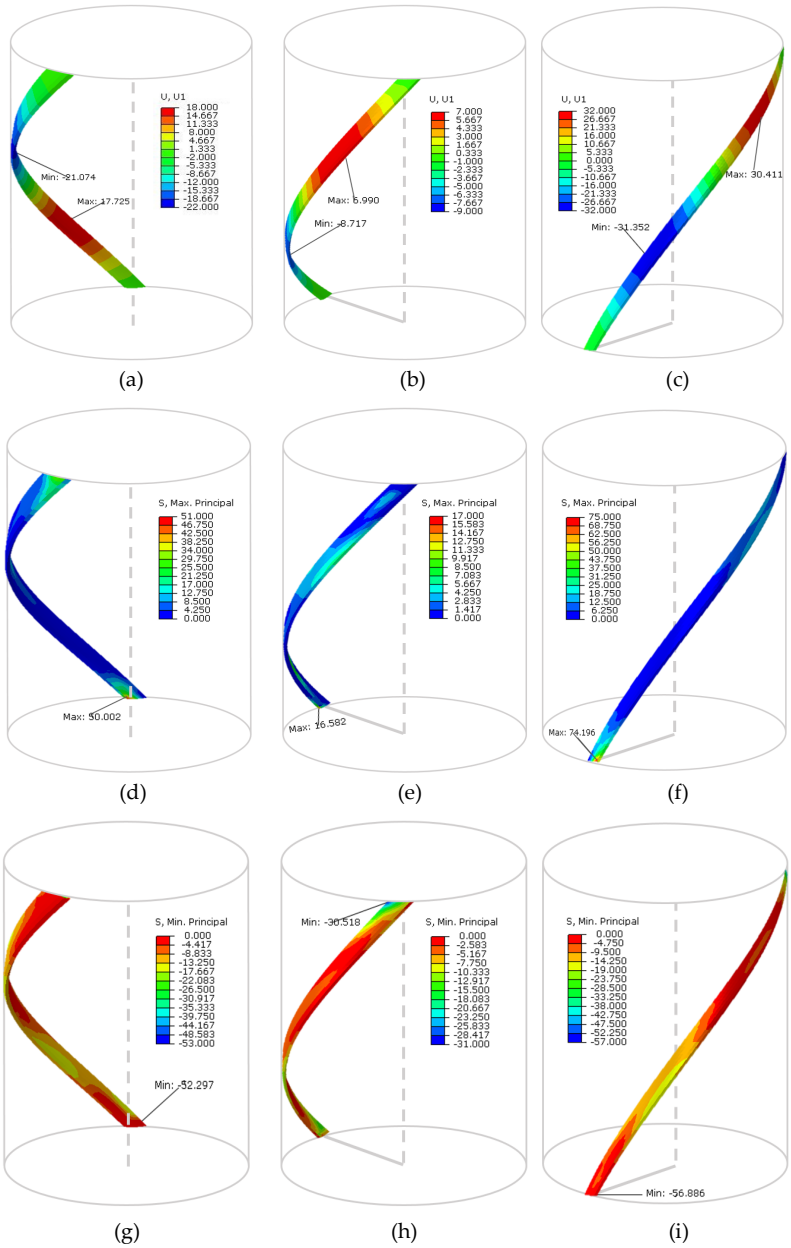

Fig. 15. Comparing of deflection in the radial direction (First row), maximum principal stress (Second row) and minimum principal stress (Third row) at different blade position; (a), (d) and (g): $\theta_0 = 0^o$, (b), (e) and (h):$\theta_0 = 60^o$, (c), (f) and (i) : $\theta_0 = 120^o$

TABLE III
MAXIMUM DEFLECTION AND MAXIMUM AND MINIMUM PRINCIPAL STRESSES FOR VARIOUS LOADING CASE

Load case	Blade Position	Maximum principal stress (MPa)	Minimum principal stress (MPa)	Maximum inwards deflection (mm)	Maximum outwards deflection (mm)
Load case 1	$\theta_0 = 0^o$	50.00	52.30	21.07	17.72
Load case 2	$\theta_0 = 60^o$	16.58	30.52	8.72	6.99
Load case 3	$\theta_0 = 120^o$	74.20	56.88	31.35	30.41

that the composite material provides sufficient stiffness for efficient turbine performance.

Fig. 15 (b) and (c) illustrate the maximum and minimum principal stresses state in the blade for three blade positions. Highest stress concentrations are computed in the region of the end-constraints in all cases, indicating that the highest risk of material fracture and fatigue failure occurs at these locations. The peak value of maximum principal stress (50 MPa) is near the bottom end-constraint for the case of $\theta_0 = 0^o$. While this value is significantly lower than the ultimate tensile stress of the material (900 MPa), a detailed design of the end-constraint will include contact between bolts and the composite material, generating significant stress magnification.

V. CONCLUSION

A modified BEMT has been developed for the analysis of curved turbine blade designs. We use this analysis tool to investigate the performance of helical bladed turbines. Our analysis reveals that the helix angle of the blade has a pronounced effect on turbine performance.

An increase in the helix angle leads to a reduction in fluctuations in torque and power output, with important implications for potential fatigue failure of blades. Our modified BEMT analysis uncovers a complex pattern of non-uniform distributed loads on turbine blades during operational conditions. A finite element structural analysis of the blade under such complex loading conditions was performed, assuming that the blade is manufactured as a multi-layered glass fibre composite lay-up. Our analysis reveals that this material is sufficiently stiff such that computed deflections are three orders of magnitude lower than the turbine radius. Maximum stress concentrations are shown to occur near to the end-constraints at the top and bottom of the blade. Follow-on analyses will identify optimal blade helix angles to maximise power-output while minimising blade deflection. Additionally, advanced finite element analysis incorporating cohesive zone fracture models will be implemented to design end-constraint fixtures so that risk of fracture and fatigue failure of the blade is minimised.

APPENDIX A: CLASSICAL BEMT MODEL

In the classic BEMT model, the relative velocity (W) and the angle of attack (α) are determined through the following equations:

$$W = \sqrt{(U_a \sin\theta)^2 + (U_a \cos\theta + R\omega)^2} \quad (22)$$

$$\alpha = tan^{-1}\left(\frac{a \sin\theta}{a \cos\theta + TSR}\right) \quad (23)$$

where U_a is the induced velocity, θ is the azimuthal angle, R is the turbine radius, ω is the angular velocity and TSR is the tip-speed-ratio. These two equations can be used for both upstream and downstream by considering the related induction factors (a).

The main hydrodynamic forces acting on the blades of a vertical axis tidal turbine are the lift and drag forces. The lift force is perpendicular to the direction of the relative velocity, while the drag force is parallel to the direction of the relative velocity (Fig. 2). The magnitude of these forces depends on the velocity of the fluid, the angle of attack of the blades, and the shape and size of the blades.

These forces can be obtained from (24) and (25) as follows, in which ρ is density, A is the area of each element, C_L and C_D are lift and drag coefficients, respectively.

$$F_L = \frac{1}{2}\rho C_L A W^2 \quad (26)$$

$$F_D = \frac{1}{2}\rho C_D A W^2 \quad (27)$$

The forces acting on the blade can also be written in terms of normal and tangential forces as follows:

$$F_T = F_L \sin\alpha - F_D \cos\alpha \quad (28)$$

$$F_N = F_L \cos\alpha + F_D \sin\alpha \quad (29)$$

REFERENCES

[1] C. Zhang, S. C. Kramer, A. Angeloudis, J. Zhang, X. Lin, and M. D. Piggott, "Improving tidal turbine array performance through the optimisation of layout and yaw angles," *International Marine Energy Journal*, vol. 5, no. 3, pp. 273-280, 2022.

[2] W. Finnegan, R. Allen, C. Glennon, J. Maguire, M. Flanagan, and T. Flanagan, "Manufacture of high-performance tidal turbine blades using advanced

composite manufacturing technologies," *Applied Composite Materials,* pp. 1-26, 2021.

[3] M. Fereidoonnezhad, M. Tahani, and V. Esfahanian, "Analysis of Ducted Wind Turbine using Surface Vorticity Method," presented at the *3rd International Conference of IEA Technology and Energy Management*, Tehran, Iran, 2017.

[4] T. Flanagan, J. Maguire, C. Brádaigh, P. Mayorga, and A. Doyle, "Smart affordable composite blades for tidal energy," in *Proceedings of the 11th European Wave and Tidal Energy Conference EWTEC2015*, 2015, pp. 6-11.

[5] B. Kirke, "Tests on ducted and bare helical and straight blade Darrieus hydrokinetic turbines," *Renewable Energy,* vol. 36, no. 11, pp. 3013-3022, 2011.

[6] B. Mannion, S. B. Leen, and S. Nash, "Development and assessment of a blade element momentum theory model for high solidity vertical axis tidal turbines," *Ocean Engineering,* vol. 197, p. 106918, 2020.

[7] S. C. Heavey, P. J. McGarry, and S. B. Leen, "Analytical Modelling of a Novel Tidal Turbine," in *The 26th International Ocean and Polar Engineering Conference*, 2016, ISOPE-I-16-295.

[8] S. C. Heavey, S. B. Leen, and J. P. McGarry, "Hydrodynamic design and analysis of a novel vertical axis turbine," *International Journal of Offshore and Polar Engineering,* vol. 28, no. 04, pp. 393-401, 2018.

[9] S. C. Heavey, S. B. Leen, and P. J. McGarry, "An efficient computational framework for hydrofoil characterisation and tidal turbine design," *Ocean Engineering,* vol. 171, pp. 93-107, 2019.

[10] B. Mannion, V. McCormack, S. B. Leen, and S. Nash, "A CFD investigation of a variable-pitch vertical axis hydrokinetic turbine with incorporated flow acceleration," *Journal of Ocean Engineering and Marine Energy,* vol. 5, no. 1, pp. 21-39, 2019.

[11] B. Mannion, S. B. Leen, and S. Nash, "A two and three-dimensional CFD investigation into performance prediction and wake characterisation of a vertical axis turbine," *Journal of Renewable and Sustainable Energy,* vol. 10, no. 3, p. 034503, 2018.

[12] W. Finnegan, E. Fagan, T. Flanagan, A. Doyle, and J. Goggins, "Operational fatigue loading on tidal turbine blades using computational fluid dynamics," *Renewable Energy,* vol. 152, pp. 430-440, 2020.

[13] B. Mannion, V. McCormack, C. Kennedy, S. B. Leen, and S. Nash, "An experimental study of a flow-accelerating hydrokinetic device," *Proceedings of the Institution of Mechanical Engineers, Part A: Journal of Power and Energy,* vol. 233, no. 1, pp. 148-162, 2019.

[14] H. Glauert, *The elements of aerofoil and airscrew theory*. Cambridge University Press, 1983.

[15] R. Templin, "Aerodynamic performance theory for the NRC vertical-axis wind turbine," National Aeronautical Establishment, Ottawa, Ontario (Canada), 1974.

[16] A. Gorlov, "Unidirectional helical reaction turbine operable under reversible fluid flow for power systems.," 1995.

[17] D. Han, Y. G. Heo, N. J. Choi, S. H. Nam, K. H. Choi, and K. C. Kim, "Design, fabrication, and performance test of a 100-w helical-blade vertical-axis wind turbine at low tip-speed ratio," *Energies,* vol. 11, no. 6, p. 1517, 2018.

[18] S. Pongduang, C. Kayankannavee, and Y. Tiaple, "Experimental investigation of helical tidal turbine characteristics with different twists," *Energy Procedia,* vol. 79, pp. 409-414, 2015.

[19] P. K. Talukdar, V. Kulkarni, and U. K. Saha, "Field-testing of model helical-bladed hydrokinetic turbines for small-scale power generation," *Renewable Energy,* vol. 127, pp. 158-167, 2018.

[20] M. H. Khanjanpour and A. A. Javadi, "Optimization of the hydrodynamic performance of a vertical Axis tidal (VAT) turbine using CFD-Taguchi approach," *Energy Conversion and Management,* vol. 222, p. 113235, 2020.

[21] U. Divakaran, A. Ramesh, A. Mohammad, and R. K. Velamati, "Effect of helix angle on the performance of helical vertical axis wind turbine," *Energies,* vol. 14, no. 2, p. 393, 2021.

[22] R. Kumar and S. Sarkar, "Effect of design parameters on the performance of helical Darrieus hydrokinetic turbines," *Renewable and Sustainable Energy Reviews,* vol. 162, p. 112431, 2022.

[23] K. B. Reddy, A. C. Bhosale, and R. Saini, "Performance parameters of lift-based vertical axis hydrokinetic turbines-A review," *Ocean Engineering,* vol. 266, p. 113089, 2022.

[24] P. Marsh, D. Ranmuthugala, I. Penesis, and G. Thomas, "Numerical simulation of the loading characteristics of straight and helical-bladed vertical axis tidal turbines," *Renewable energy,* vol. 94, pp. 418-428, 2016.

[25] M. Moghimi and H. Motawej, "Developed DMST model for performance analysis and parametric evaluation of Gorlov vertical axis wind turbines," *Sustainable Energy Technologies and Assessments,* vol. 37, p. 100616, 2020.

[26] J. H. Strickland, "Darrieus turbine: a performance prediction model using multiple streamtubes," Sandia Labs., Albuquerque, N. Mex.(USA), 1975.

[27] I. Paraschivoiu, "Double-multiple streamtube model for Darrieus in turbines," *NASA. Lewis Research Center Wind Turbine Dyn.,* 1981.

[28] M. Rossander *et al.*, "Evaluation of a blade force measurement system for a vertical axis wind turbine using load cells," *Energies,* vol. 8, no. 6, pp. 5973-5996, 2015.

[29] S. Brusca, R. Lanzafame, and M. Messina, "Design of a vertical-axis wind turbine: how the aspect ratio affects the turbine's performance," *International Journal of Energy and Environmental Engineering,* vol. 5, pp. 333-340, 2014.

[30] P. Brøndsted, J. W. Holmes, and B. F. Sørensen, "Wind rotor blade materials technology," *European sustainable energy review,* no. 2, pp. 36-41, 2008.

[31] D. M. Grogan, S. B. Leen, C. R. Kennedy, and C. Ó. Brádaigh, "Design of composite tidal turbine blades," *Renewable Energy,* vol. 57, pp. 151-162, 2013.

[32] O. Oguclu, "Structural Design and Stress Analysis of a Helical Vertical Axis Wind Turbine Blade," *Sakarya University Journal of Science,* vol. 24, no. 6, pp. 1151-1161, 2020.

[33] W. Finnegan, Y. Jiang, N. Dumergue, P. Davies, and J. Goggins, "Investigation and validation of numerical models for composite wind turbine blades," *Journal of Marine Science and Engineering,* vol. 9, no. 5, p. 525, 2021.